

Emergence of directed motion in a crowded suspension of overdamped particles with different effective temperatures

Deborah Schwarcz^{1,*} and Stanislav Burov^{2,†}

¹*Department of Mathematics, Bar-Ilan University, Ramat Gan 5290002, Israel*

²*Physics Department, Bar-Ilan University, Ramat Gan 5290002, Israel*



(Received 21 March 2022; accepted 13 October 2023; published 12 February 2024)

In this work, we focus on the behavior of a single passive Brownian particle in a suspension of passive particles with short-range repulsive interactions and higher effective temperature. While the forces affecting the single particle are thermal-like fluctuations and repulsion, due to other particles in the suspension, our numerical simulations show that on intermediate timescales directed motion on a single-particle level emerges. This emergent directional motion leads to a breakdown of the Einstein relation and nonmonotonic augmentation of the measured diffusion coefficient. Directional tendency increases with the density of the suspension and leads to growth of the diffusivity with the density of the suspension, a phenomenon recently observed for a system of hard spheres by Ilker, Castellana, and Joanny. Counterintuitively, the directional flow originates from the tendency of different particles to push each other out of their way. Due to such strictly repulsive interactions, nearby particles form into temporally correlated pairs and move cooperatively, thus creating a preferred direction of motion on intermediate timescales. We show that directional motion emerges when the ratio of the effective temperatures of the tracked particle and suspension constituents is below a critical value.

DOI: [10.1103/PhysRevResearch.6.013156](https://doi.org/10.1103/PhysRevResearch.6.013156)

I. INTRODUCTION

Active particles are defined by the ability to perform directed motion while consuming energy from the environment and dissipating it back [1–4]. This signature of directional transport of active particles contrasts with the passive motion of Brownian particles, which are driven by thermal fluctuations. Active matter, like the cytoskeleton, relies on the presence of systematic motion of the basic ingredients, e.g., molecular motors [5]. The presence of directionality in the movement can be exploited; for example, bacteria’s run and tumble property was utilized to operate micromachines [6,7]. Heat engines that are designed to use fluctuations on a single-particle level [8–10] experience an increase in efficiency when the surrounding reservoir includes active ingredients [11]. While active particles are naturally present in the biological world, e.g., bacteria and molecular motors, numerous artificial examples are based on chemical reactions [1] or manipulation by external fields [12]. For example, directed propulsion can be achieved for Janus spherical particles by unequally coating the surface with platinum [13]. In this work we focus on the appearance of directional motion for overdamped passive Brownian particles.

The appearance of macroscopic and asymmetric space-time states (namely, directional flows) was the focus of the dissipative structures theory [14]. The most frequently used example of a dissipative structure is the Rayleigh-Bénard instability [15] where macroscopic convection starts when a critical temperature difference of the confining plates is reached. The existence of a point, beyond which a novel nonequilibrium dynamic state is formed, is the sole idea behind dissipative structures on the macroscale. Does such point exist when a single particle (SP) is considered? Can directed motion of a SP, be an emergent phenomenon when a passive Brownian particle (PBP) is pushed far enough into the nonequilibrium realm of a thermal system? Namely, can a sufficient difference between the effective temperature of the SP and other constituents of the suspension be a trigger for directional motion of the SP? In theoretical studies of binary mixtures of PBPs with different temperatures, a demixing transition (for sufficiently high concentration) was observed [16,17]. Such demixing into phases with low and high temperature resembles the motility-induced phase separation to slow and fast active particles present in active systems [18]. Moreover, a system consisting of two particles in contact with different thermostats and a binding potential reaches a steady state that does not satisfy Boltzmann statistics [16,19–21]. The nonequilibrium properties of two PBPs in contact with different thermostats, and pairwise quadratic interactions, were utilized to identify broken detailed balance on a mesoscopic scale [22] and to quantify dissipation [23]. Nonequilibrium steady states were also studied when three PBPs with different temperatures are considered [24]. It was shown that PBPs with higher diffusivity (“hot” particles) effectively attract each other when immersed in a suspension of

*deborah.schwarcz@gmail.com

†stasbur@gmail.com

Published by the American Physical Society under the terms of the Creative Commons Attribution 4.0 International license. Further distribution of this work must maintain attribution to the author(s) and the published article’s title, journal citation, and DOI.

PBPs with lower diffusivity (“cold” particles) [25]. Moreover, the effective temperature of a “hot” tracer decreases due to interaction with a bath of “cold” particles [26]. Recently, it was found that the long-time diffusivity of a single cold PBP in a solution of hot PBPs, increases as a function of hot PBPs self-diffusivity and density [27,28].

In this paper, we explore the microscopic mechanism that leads to the enhancement of the long-time diffusion coefficient of a cold PBP in a bath of hot PBPs. We observe that once the temperature, i.e., self-diffusion coefficient, ratio of the cold and hot PBPs crosses a specific value, a presence of directional motion appears in the transport of the cold PBP. The timescales when the cold PBP moves in a directed fashion depend on the density of the surrounding particles. Our numerical simulations show a rich behavior of the tracked SP. We reveal a transition to directed motion, breakdown of the Einstein relation, and nonmonotonic behavior of the long-time diffusion coefficient as a function of the density of the solution.

The paper is organized as follows: In Sec. II we present our model: a two-dimensional suspension of hot PBPs and a single cold PBP that is immersed into this suspension. In Sec. III, we analyze the mean-square displacement of the cold PBP and demonstrate the enhancement of the long-time diffusion coefficient. In Sec. IV, we utilize the behavior of the distribution of the relative angle of the cold PBP to observe the appearance of directed motion. In Sec. V we show that the cold PBP tends to interact with a single hot PBP, i.e., nearest neighbor, forming a temporarily correlated pair. Our findings strongly suggest that the spontaneous directional symmetry breaking of cold PBPs is associated with the formation of such temporarily correlated pairs. The discussion and summary of our findings are provided in Sec. VI.

II. THE MODEL

We perform simulations of a two-dimensional solution of PBPs. The position of every particle i , \vec{r}_i , is governed by the overdamped Langevin equation [29]

$$\frac{d\vec{r}_i}{dt} = \frac{1}{\gamma} \sum_j \vec{F}(r_{i,j}) + \sqrt{2D_i} \vec{\eta}_i(t), \quad (1)$$

where $\vec{F}(r_{i,j})$ is the force due to interaction with particle j and $r_{i,j} = |\vec{r}_i - \vec{r}_j|$ is the distance between particle i and particle j . D_i is the diffusion coefficient of particle i and $\vec{\eta}_i(t) = \eta_i^x \hat{x} + \eta_i^y \hat{y}$, while η_i^x (and η_i^y) is the random δ -correlated Gaussian noise, i.e., the integral $\int_0^t \eta_i(t') dt'$ is the Wiener process $W_i(t)$ where $\langle W_i(t) W_j(t') \rangle = \delta_{i,j} \min(t, t')$ and $\langle W_i(t)^2 \rangle = t$. The infinitesimal increment of $W_i(t)$, $W_i(t + dt) - W_i(t) = \Omega(t) \sqrt{dt}$, is used to implement the Euler-Maruyama integration scheme, where $\Omega(t)$ is a zero-mean Gaussian process with unit variance [30]. Coefficient $1/\gamma$ plays the role of inverse friction coefficient, and in this work, we use $\gamma = 1$. The force $\vec{F}(r_{i,j})$ is determined by the Weeks-Chandler-Andersen (WCA) potential [31] (the purely repulsive part of the Lennard-Jones potential):

$$V_{i,j} = \begin{cases} 4\epsilon[(\sigma/r_{i,j})^{12} - (\sigma/r_{i,j})^6], & r_{i,j} \leq 2^{1/6}\sigma \\ 0, & r_{i,j} > 2^{1/6}\sigma. \end{cases} \quad (2)$$

The diffusion coefficient of all the particles in the solution is D_a . A single PBP with diffusion coefficient $D_b < D_a$ is immersed into the solution. The particles in the solution and the immersed particle have the same mobility but different diffusion coefficients, hence different effective temperatures. The immersed SP has the same size as the other particles in the solution, and it interacts with other particles via similar WCA potential.

All the particles are positioned on a two-dimensional box of size $S = 20\sigma \times 20\sigma$ and periodic boundary conditions are implemented. For all particles, Eq. (1) is advanced in time by the Euler-Maruyama method while we use $\epsilon = 0.01$, $\sigma = 1$, and the discrete-time step $\delta t = 0.005$. The density of the solution, ϕ , is determined by the total number of particles with diffusion coefficient D_a in the solution, N_a ,

$$\phi = N_a \pi r_0^2 / S, \quad (3)$$

where $2 \times r_0 = 2^{1/6}\sigma$ is the minimal distance at which two particles start to repel each other. During the simulation, the position of the SP with diffusion coefficient D_b is recorded.

III. MEAN-SQUARED DISPLACEMENT

The first characteristic that we explore is the time- and ensemble-averaged mean-squared displacement (MSD), of the tracked SP (with D_b) during time frame Δ ,

$$\text{MSD}(\Delta) = \frac{1}{t - \Delta} \int_0^{t-\Delta} \langle [\vec{r}_b(t' + \Delta) - \vec{r}_b(t')]^2 \rangle dt', \quad (4)$$

where $\vec{r}_b(t')$ is the position of the tracked particle at time t' and t is the measurement time. Figure 1(a) displays $\text{MSD}(\Delta)$ for the case of $D_b/D_a = 0.1$. The MSD grows linearly for short times as $2D_b\Delta$ and experiences a transition to a diffusive behavior with a higher long-time diffusion coefficient at longer times, i.e., $\text{MSD}(\Delta) \sim 2D_b^\infty\Delta$, where $D_b^\infty/D_b = 2.2$ for the particular case of Fig. 1(a). The MSD enhancement is fitted by a phenomenological formula for the MSD of an active particle [1,13]:

$$\text{MSD}(\Delta) = [2D_b + A]\Delta + AB[e^{-\Delta/B} - 1], \quad (5)$$

where A and B are constants [see Supplemental Material (SM) [32] for further details].

The increase of diffusion of a cold particle (low diffusion coefficient) moving between hot particles (high diffusion coefficient) was previously observed [27,28]. In these previous studies, a system of hard spheres [27] and a system of soft particles [28] were used. In [27] the diffusion was enhanced when the ratio of the diffusivity of slow particles and the diffusivity of fast particles was below $1/3$ (see also [28]). Our results [Fig. 1(b)] support these findings for sufficiently low ϕ . We note that enhancement of transport was recently observed in active systems as well [33,34]. Several questions are in place. What is the microscopical mechanism that leads to such enhancement of effective diffusion coefficient? Is the observed enhancement of the diffusion coefficient also associated with directional motion? While the increase in MSD can occur due to a series of large and uncorrelated “kicks”/bombardments [35] (see SM for additional details), it is also possible that the microscopic mechanism leads to a directed, activelike motion. Finally, what happens to the effect when the density of the

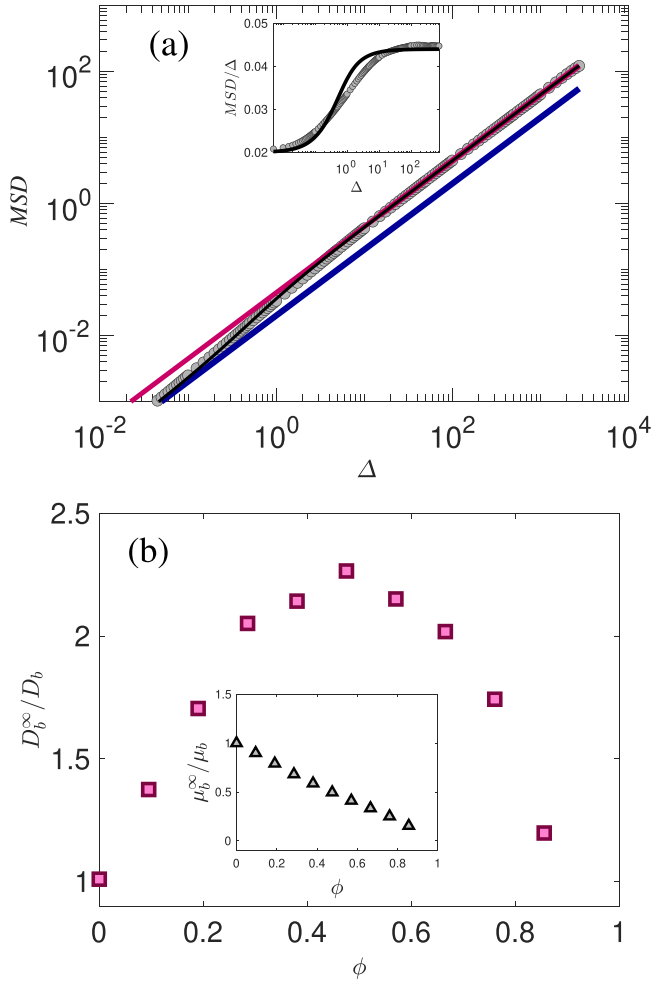


FIG. 1. (a) MSD of a SP with self-diffusion coefficient $D_b = 0.01$ in a solution of PBPs with $D_a = 0.1$, while the density $\phi = 0.47$. Gray circles represent simulated data, the blue line represents short period diffusion $2D_b\Delta$. The pink line represents long-time diffusion $2D_b^\infty$, where the logarithmic time diffusion coefficient is $D_b^\infty = 0.022$. The black line represents the fit to the MSD of an active particle, Eq. (5), where $A = 0.0245$ and $B = 0.375$. Inset: MSD/ Δ with parameters of panel (a) and semilogarithmic scale. The black line represents the fit to the MSD of an active particle. (b) D_b^∞/D_b as a function of the density of the solution. The squares represent the calculation of D_b^∞ via the MSD of unperturbed SP [Eq. (4)]. Inset: The measured mobility $\mu_b^\infty = v_d/F$ of the SP measured at different densities, divided by the mobility μ_b measured at $\phi = 0$. v_d is the measured terminal velocity of the SP measured for external force; the value $F = 0.1$ was used. For both panels 6×10^5 simulation steps were performed. Averaging over time and 40 ensembles was performed.

suspension is further increased? We address these questions below.

When the long-time effective coefficient D_b^∞ is measured for different values of the suspension density ϕ , a nonmonotonic dependence is observed [Fig. 1(b)]. D_b^∞ increases with ϕ up to $\phi \approx 0.45$, i.e., crowded is faster. Similar behavior for different ratios of diffusion coefficients is presented in Fig. S1(a) in the SM. Recently, diffusion enhancement via crowding was observed for an active system of strongly inter-

acting stiff self-propelled filaments [36] and enzyme diffusion driven by chemical reactions [37–40]. For PBP, D_b^∞ will stop increasing for sufficiently high solution density. The intuitive reduction of D_b^∞ as a function of density appears when $\phi \gtrsim 0.45$. Such nonmonotonous behavior of the diffusion coefficient was observed in glassy systems [41–44]. The cause of the eventual decrease of the long-time diffusion coefficient, and therefore the overall nonmonotonic behavior, is the cage effect: an obstruction of motion due to nearby particles that lead to the appearance of negative correlation of displacements [45].

In addition to the described extraction of the diffusion coefficient by measurement of the MSD of unperturbed particles, we calculate the mobility of the cold SP. A small external force F was applied on the SP and the long-time drift velocity v_d was measured. The mobility, $\mu_b^\infty = v_d/F$, was found to monotonically decrease with growing ϕ , as is intuitively expected for a growing crowdedness of the system [see the inset in Fig. 1(b)]. The difference between the behavior of the long-time diffusion coefficient and the mobility shows that the Einstein relation is broken. Such failure of the Einstein relation is a signature of the nonequilibrium state of our system (see also [46]).

IV. RELATIVE ANGLE

To answer the question whether the enhancement is accompanied by directed motion, we search for directional properties in the motion of the PBP with $D = D_b$ and use the correlations between successive displacements [45,47,48]. Specifically, we use the distribution of directional change by employing the relative angle $\theta(t; \Delta)$ [49], previously utilized for analysis of myosin dynamics [49], Lagrangian trajectories in turbulence [50], swarming bacteria [51], football players [52], and active Brownian particles [53]. θ is the angle between two successive steps of time span Δ performed by the tracked SP:

$$\cos \theta(t; \Delta) = \frac{\vec{v}_b(t; \Delta) \cdot \vec{v}_b(t + \Delta; \Delta)}{|\vec{v}_b(t; \Delta)| |\vec{v}_b(t + \Delta; \Delta)|}, \quad (6)$$

where $\vec{v}_b(t; \Delta) = \vec{r}_b(t + \Delta) - \vec{r}_b(t)$. For a given Δ , $\theta(t; \Delta)$ is computed for all different t 's in a trajectory. $P(\theta; \Delta)$ is the distribution of directional change obtained for all $0 \leq \theta \leq \pi$. The $P(\theta; \Delta)$ of a noninteracting PBP attains a uniform shape [Fig. 2(a)], for any lag times Δ , since every step is independent of the other steps. There is a preference for the retraction of steps when the particle is caged and Δ is large enough. In such case $P(\theta; \Delta)$ will have a peak at $\theta = \pi$ [Fig. 2(a)]. When there is a directed motion, $P(\theta; \Delta)$ will show a peak at $\theta = 0$ for Δ 's that correspond to timescales for which directionality exists [49]. The peak at $\theta = 0$ means that if the particle moved for a lag time Δ in the direction of \vec{a} , for the next Δ , the preferred direction of motion will be again \vec{a} . In Fig. 2(a) the $P(\theta; \Delta)$ is plotted for three different values of the density ϕ of the solution. When $\phi = 0$, $P(\theta; \Delta)$ is uniform as is expected for a noninteracting PBP. When ϕ is sufficiently large, a peak at $\theta = \pi$ is observed, as is expected for a particle caged by its neighbors. Finally, there is a regime when the solution is not very dense, and $P(\theta; \Delta)$ peaks at $\theta = 0$. For example, when $\phi = 0.47$ [see Fig. 2(a)]. The PBP has not simply performed

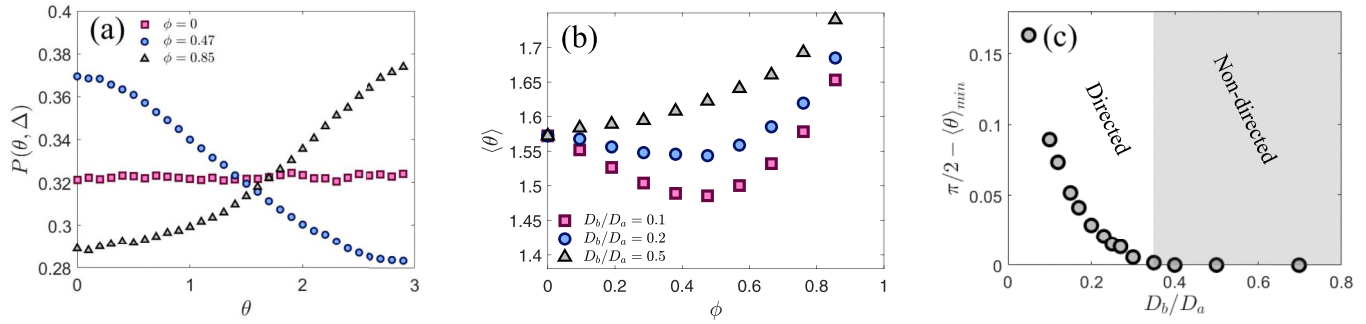


FIG. 2. (a) Relative angle distribution $P(\theta; \Delta)$ for the SP with $D = D_b$. Three different solution densities ϕ are presented: $\Delta = 200\delta t$, $D_a = 0.1$, and $D_b = 0.01$. (b) Mean relative angle $\langle \theta \rangle$ of the tracked SP as a function of ϕ for three different ratios of D_b/D_a ($\Delta = 200\delta t$). Values of $\langle \theta \rangle < \pi/2$ correspond to directed motion. (c) Phase diagram of directed vs uncorrelated motion of the tracked SP. For every D_b/D_a the minimal value of $\langle \theta \rangle$ ($\langle \theta \rangle_{\min}$) was found (searched for different Δ 's and ϕ). $\pi/2 - \langle \theta \rangle_{\min} = 0$ states that the behavior is passive, when $\pi/2 - \langle \theta \rangle_{\min} > 0$ directed motion is observed. When $D_b/D_a > 0.3$ the correlations were either nonexistent or negative, therefore the zero value of the parameter $\pi/2 - \langle \theta \rangle_{\min} \cdot D_a$ was always set to 0.1. For all panels, 6×10^5 simulation steps were recorded, and averaging over 50 ensembles was performed.

bigger jumps that increased the MSD; it moved in a directed style for a period 2Δ .

The behavior of the relative angle also reveals that directional motion emerges only if the ratio D_b/D_a is sufficiently smaller than 1. The behavior of $\langle \theta(\Delta) \rangle = \int_0^\pi \theta P(\theta; \Delta) d\theta$ can be utilized as a measure of the directional motion. When the motion is uncorrelated and nondirectional, the distribution of θ is uniform [Fig. 3(a)] therefore $\langle \theta \rangle = \pi/2$. In Fig. 2(b) we present $\langle \theta \rangle$ as a function of ϕ for three different values of D_b/D_a . When $\langle \theta \rangle$ attains values below $\pi/2$ it means that $P(\theta; \Delta)$ is peaked around $\theta = 0$ and the particle moves directionally for a time frame of 2Δ . Alternatively, when $\langle \theta \rangle > \pi/2$, $P(\theta; \Delta)$ is peaked around $\theta = \pi$, and the particle is caged. Therefore, directed motion emerges when the minimum measured $\langle \theta \rangle$, i.e., $\langle \theta \rangle_{\min}$, is smaller than $\pi/2$. Figure 2(b) displays a monotonic growth of $\langle \theta \rangle$ as a function of ϕ when $D_b/D_a = 0.5$. Such behavior is what is naively expected from a system that becomes more and more crowded, and SP becomes increasingly caged [45]. On the other hand, for small enough D_b/D_a , $\langle \theta \rangle$ behaves nonmonotonically as a function of ϕ , with minimum values below $\pi/2$. We use $\pi/2 - \langle \theta \rangle_{\min}$ as an order parameter for the directed mo-

tion of the tracked SP. When the movement is nondirected, i.e., the displacement is either noncorrelated or negatively correlated, $\pi/2 - \langle \theta \rangle_{\min}$ is always 0. When directed motion occurs this parameter can produce nonzero values. For a given D_b/D_a , $\langle \theta \rangle_{\min}$ is calculated for all different Δ 's and ϕ 's. The results are displayed in Fig. 2(c). When D_b/D_a is above ≈ 0.3 , $\pi/2 - \langle \theta \rangle_{\min}$ was always 0 and behaved similarly to the case of $D_b/D_a = 0.5$ in Fig. 2(b), irrespective of the size of Δ . We conclude that no directed motion is detected when $D_b/D_a > 0.3$. For $D_b/D_a < 0.3$, a minimum value of $\langle \theta \rangle_{\min}$ was always found to be below $\pi/2$ and $\langle \theta \rangle$ behaves similarly to the cases $D_b/D_a = 0.2$ and $D_b/D_a = 0.1$ in Fig. 2(b). Therefore for $D_b/D_a < 0.3$ there is always a time span Δ for which the PBP moves in a directed fashion. In Fig. S1 of the SM we show that the long-time diffusion coefficient D_b^∞ is also enhanced when $D_b/D_a < 0.3$. Therefore a sufficiently low ratio of diffusivities is needed in order to obtain directed motion which gives rise to the enhancement of the diffusion coefficient. This enhancement of the diffusion coefficient of a cold particle in a bath of hot particles was previously observed [27,28]. Our observation is in line with the original statement of [27] where it was predicted that the

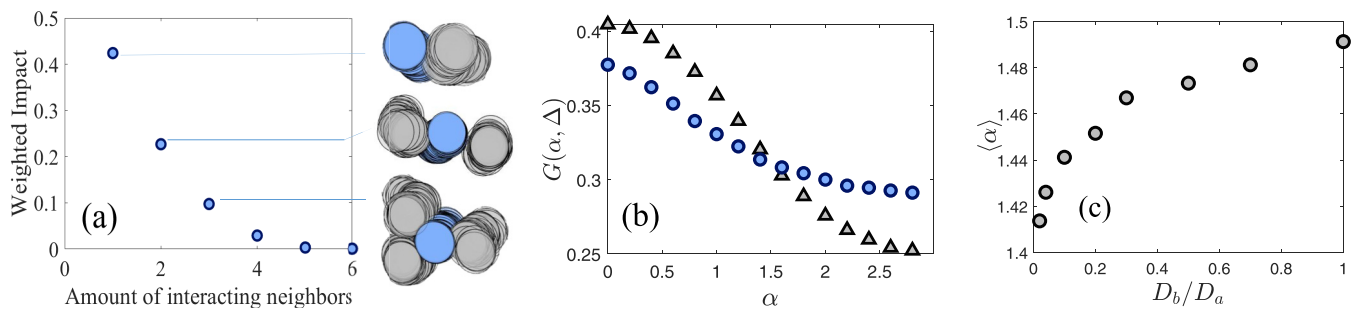


FIG. 3. (a) Weighted impact: The portion of temporal span Δ during which the tracked SP simultaneously interacted with n particles, as a function of $n = 1, 2, 3, 4, 5, 6$. $D_a = 0.1$, $D_b = 0.01$, $\phi = 0.475$, and $\Delta = 200\delta t$. (b) $G(\alpha; \Delta)$: The probability density function of the angle $\alpha(t; \Delta)$ [Eq. (7)] between the direction traced by the tracked SP during Δ and the direction traced by a particle with which the tracked SP mostly interacted during Δ . Such two particles form a temporally correlated pair. $\Delta = 200\delta t$ and two ratios of $D_b/D_a = 1$ (\circ), $D_b/D_a = 0.2$ (\triangle) are presented. (c) Average $\alpha(t; \Delta)$ ($\langle \alpha \rangle$) as obtained from $G(\alpha; \Delta)$ in panel (b). 6×10^5 simulation steps and averaging over 40 ensembles was performed.

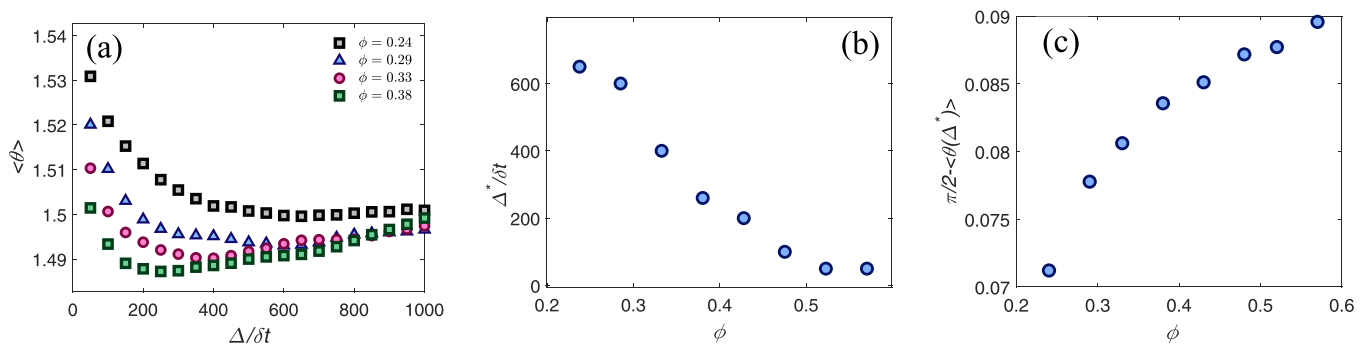


FIG. 4. (a) Nonmonotonic evolution of the mean relative angle $\langle \theta \rangle$ as a function of Δ for four different densities. (b) Δ^* is the Δ for which the minimum value of $\langle \theta \rangle$ was obtained [see panel (a) for a given ϕ and D_b/D_a]. Plotted as a function of the suspension density ϕ . (c) Order parameter $\pi/2 - \langle \theta \rangle$, when the mean relative angle $\langle \theta \rangle$ is computed at $\Delta = \Delta^*$ [panel (b)]. Higher values of the order parameter describe more pronounced directed motion. For all panels, $D_a = 0.1$ and $D_b = 0.01$; 6×10^5 simulation steps and averaging over 100 ensembles was performed.

long-time diffusion coefficient of a tracer particle increases if the ratio of temperatures, i.e., D_b/D_a , is smaller than $1/3$. The presented analysis of relative angle reveals the reason for the enhancement: at intermediate timescales during which the cold particle moves persistently and experiences a memory of the traced direction. At sufficiently long timescales this memory is lost and the effective displacements become uncorrelated. But since on intermediate timescales the motion was directed, i.e., positively correlated, these effective uncorrelated displacements are larger, in size, as compared to displacements on smaller timescales. This increase in the size of a single uncorrelated displacement leads to the observed enhancement of the long-time diffusion coefficient. Therefore we can state that the observed directed motion on intermediate timescales leads to the enhancement of the diffusion coefficient on long timescales. In the next section, we address the mechanism that is responsible for the observed spontaneous directional symmetry breaking, i.e., directional motion.

V. TEMPORALLY CORRELATED PAIRS

To elucidate the origin of directional motion, we measure the fraction of time that the traced SP spent simultaneously interacting with 1, 2, 3, ..., neighbors. The weighted impact is the portion of time Δ that the SP simultaneously interacted (i.e., experienced nonzero force) with a number of other PBPs. Panel (a) of Fig. 3 shows that the majority of the interactions are two-body encounters. We focus on two-particle encounters and define the angle α :

$$\cos \alpha(t; \Delta) = \frac{\vec{v}_b(t; \Delta) \cdot \vec{v}_a(t + \Delta; \Delta)}{|\vec{v}_b(t; \Delta)| |\vec{v}_a(t + \Delta; \Delta)|}, \quad (7)$$

i.e., the angle between the displacement of the tracked SP during Δ and the displacement of a neighbor SP with which it mostly interacted during Δ . We tally the interactions between the tracked SP and each of its neighbors and then compute the value of α while using the neighbor SP with whom the tracked SP had the highest number of interactions during Δ . When particles do not interact with each other, the probability density function of $G(\alpha, \Delta)$ is uniform, as one would expect for a typical PBP. However, if there is a peak in the probability density function of $G(\alpha, \Delta)$ around $\alpha = 0$, it suggests that

the particles tend to move in the same direction. On the other hand, if the peak is at $\alpha = \pi/2$, this indicates that the particles tend to move in opposite directions. Figure 3(b) displays the probability density function of α , $G(\alpha, \Delta)$, computed for all possible displacements of the tracked SP along the trajectory. Even when $D_b = D_a$, the distribution $G(\alpha, \Delta)$ is peaked at $\alpha = 0$. Meaning that there are timescales when two neighbors prefer to move in the same direction (on average), even when their temperatures are equal. This effect is achieved due to the presence of other PBPs in the vicinity of the pair. These PBPs do not let particles in the pair separate and create effective temporal coupling for the pair. We term such a pair a temporally correlated pair (TCP). When we decrease the fraction D_b/D_a , this effect of correlated motion of neighbor particles is enhanced. Panel (c) of Fig. 3 shows how the average α is decreasing with decreasing D_b/D_a . The preference to move in a cohort manner increases when $D_b/D_a \rightarrow 0$.

This phenomenon of TCP creation is what leads to spontaneous directional symmetry breaking. On intermediate timescales, the preferred direction of motion becomes the line of interaction between the constituents of the TCP pair. In Fig. 4(a) we plot the temporal evolution of the average relative angle $\langle \theta \rangle$ as a function of Δ . The lower the value of $\langle \theta \rangle$, the greater the directional preference of the motion. $\langle \theta \rangle$ behaves nonmonotonically with Δ . It decreases for short and intermediate timescales and grows when Δ is sufficiently large. Since the interaction between the different SPs is purely repulsive, it takes time for the effective interaction, which involves the surrounding particles in the suspension, to build up and create a TCP. Therefore the decrease of $\langle \theta \rangle$ on short timescales. A given TCP cannot survive for a very long time since the role of the partner with which a given SP interacts the most will switch from one particle to another. This leads to the observed growth of $\langle \theta \rangle$ for large Δ . We call the Δ for which $\langle \theta \rangle$ obtains its minimal value, Δ^* , and associate it with the average lifetime of a TCP. Δ^* is the timescale on which the SP moves most persistently in a specific direction defined by the orientation of the TCP. For Δ 's smaller/larger than Δ^* $\langle \theta \rangle$ is closer to $\pi/2$, meaning the motion is less directional, which occurs due to switching of most interacting partners and breaking of the TCP. We expect two different behaviors of Δ^* and $\langle \theta(\Delta^*) \rangle$ as a function of the density of

the suspension ϕ . (i) The denser the suspension, the faster the effective interaction will build up and cause the faster formation of TCPs. But, since the suspension is denser, it will also be expected to cause a faster dissociation of partners and dissociation of TCPs. A decrease of Δ^* with ϕ is expected. (ii) The denser the suspension the closer the different SPs are; therefore, the created TCP will be tighter. Meaning, the SPs have less free space, and the directional motion will be more pronounced. This will show itself in a smaller $\langle\theta(\Delta^*)\rangle$. An increase of $\pi/2 - \langle\theta(\Delta^*)\rangle$ is expected with ϕ , i.e., the peak around $\theta = 0$ of $P(\theta, \Delta^*)$ grows with ϕ . Both (i) and (ii) are observed in Figs. 4(b) and 4(c).

The effect of the surrounding media is thus twofold. The presence of surrounding particles provides the means for directional symmetry breaking by temporal coupling of nearby particles. But exactly the same surrounding particles randomize this coupling, thus destroying the formed TCP and restoring the directional symmetry on longer timescales. A sufficiently long time Δ^* between the reorientation events is needed to observe the effect of directional motion.

VI. DISCUSSION

The results presented in this work show that directional motion on the SP level can emerge due to differences in effective temperatures. The motion of a single PBP, surrounded by other PBPs with a higher temperature becomes directed. When the density is sufficiently low, the SP with a lower temperature, i.e., lower diffusion coefficient D_b , temporally couples to one hot SP with diffusion coefficient D_a and creates a TCP. As ϕ grows, the coupling becomes more prominent, the persistence of directed motion is enhanced on intermediate timescales, and so is the long-time diffusion coefficient D_b^∞ . But this occurs only if the interactions on the TCP level are not randomized by interactions with other particles in the immediate neighborhood of the TCP. When the density ϕ is sufficiently high, the caging effect takes place, i.e., the growing peak for $\theta = \pi$ of $P(\theta, \Delta)$ (Fig. 2). The rise of caging implies that the tracked SP frequently encounters many surrounding PBPs. The lifetime of the TCP, or the time while the directional symmetry breaking holds, Δ^* , decreases with density [Fig. 4(b)]. The tracked SP simply switches partners too frequently thus effectively randomizing its motion and preventing persistence in a specific direction.

Thus the picture that emerges from our study is of effective directed motion that is a consequence of TCP creation for sufficiently prolonged time periods. While TCP can occur also when the tracked SP has exactly the same temperature as the nearby PBPs, the interaction and the cooperative motion on

the TCP level increase as the ratio of the effective temperatures decreases. The density of the suspension also facilitates the creation of TCP and the time for which a given TCP survives. While the tracked SP is a part of a given TCP it has a preferred direction of motion, dictated by the location of the other part of the TCP. Therefore, the survival time of a given TCP defines the timescale over which the motion of the tracked SP is directional. When this timescale is long enough, the effective displacements become large enough and leads to the observed enhancement of the long-time diffusion coefficient D_b^∞ . But the effect of the growth of ϕ is twofold. While the interaction on the TCP level increases, the encounters with other nearby particles become more frequent (caging effect) and so the lifetime of a given TCP will eventually start to decrease when ϕ is high enough. This leads to the diminishing of the long-time diffusion coefficient and the overall nonmonotonic behavior of D_b^∞ observed in Fig. 1.

The observed breakdown of the Einstein relation [Fig. 1(b)] is consistent with the described mechanism of enhancement of diffusion coefficient due to the spontaneous creation of TCPs. The existence of an external field (applied only upon the cold SP) and its direction is uncorrelated with the spontaneous direction that emerges due to the creation of TCP. The dragged SP already has a preferred direction of motion (i.e., the direction of the external force), and the creation of a TCP only obstructs the dynamics in this preferred direction; while for the case when no external force is present, the TCP enforces a preferred direction of motion. When an external force is applied the nearby particles (potential partners of a TCP) only “stand in the way” of the preferred direction of motion, i.e., the direction of the external force. Therefore the MSD, obtained via the Einstein relation, monotonically decays as a function of the density; unlike the observed nonmonotonic behavior of D_b^∞ with ϕ , when no external force is present.

In this work, we do not observe a macroscopic motion of many particles. Instead, we have seen that for the SP, directional motion occurs only when $D_b/D_a \lesssim 0.3$ [Fig. 2(c)], which is consistent with previous studies that observed enhancement of long-time diffusion coefficients [27,28]. On the SP level, this emergent spontaneous directional symmetry breaking can be addressed as an SP analog of dissipative structure, and D_b/D_a (i.e. the temperatures ratio) is the parameter that must be modified in order to enhance TCP creation that facilitates the directed motion of a single PBP.

ACKNOWLEDGMENT

This work was supported by the Israel Science Foundation under Grant No. 2796/20.

-
- [1] C. Bechinger, R. Di Leonardo, H. Löwen, C. Reichardt, G. Volpe, and G. Volpe, Active particles in complex and crowded environments, *Rev. Mod. Phys.* **88**, 045006 (2016).
 - [2] S. Ramaswamy, The mechanics and statistics of active matter, *Annu. Rev. Condens. Matter Phys.* **1**, 323 (2010).
 - [3] M. E. Cates, Diffusive transport without detailed balance in motile bacteria: Does microbiology need statistical physics? *Rep. Prog. Phys.* **75**, 042601 (2012).
 - [4] G. Szamel, Self-propelled particle in an external potential: Existence of an effective temperature, *Phys. Rev. E* **90**, 012111 (2014).
 - [5] M. C. Marchetti, J. F. Joanny, S. Ramaswamy, T. B. Liverpool, J. Prost, M. Rao, and R. A. Simha, Hydrodynamics of soft active matter, *Rev. Mod. Phys.* **85**, 1143 (2013).
 - [6] A. Sokolov, M. M. Apodaca, B. A. Grzybowski, and I. S. Aranson, Swimming bacteria power microscopic gears, *Proc. Natl. Acad. Sci. USA* **107**, 969 (2010).

- [7] R. Di Leonardo, L. Angelani, D. Dell'Arciprete, G. Ruocco, V. Iebba, S. Schippa, M. P. Conte, F. Mecarini, F. De Angelis, and E. Di Fabrizio, Bacterial ratchet motors, *Proc. Natl. Acad. Sci. USA* **107**, 9541 (2010).
- [8] V. Blickle and C. Bechinger, Realization of micrometre-sized stochastic heat engine, *Nat. Phys.* **8**, 143 (2012).
- [9] A. Dechant, N. Kiesel, and E. Lutz, All-optical nanomechanical heat engine, *Phys. Rev. Lett.* **114**, 183602 (2015).
- [10] I. A. Martínez, É. Roldán, L. Dinis, D. Petrov, J. M. R. Parrondo, and R. A. Rica, Brownian Carnot engine, *Nat. Phys.* **12**, 67 (2016).
- [11] S. Krishnamurthy, S. Ghosh, D. Chatterji, R. Ganapathy, and A. K. Sood, A micrometre-sized heat engine operating between bacterial reservoirs, *Nat. Phys.* **12**, 1134 (2016).
- [12] Z. Yan, S. K. Gray, and N. F. Scherer, Potential energy surfaces and reaction pathways for light mediated self-organization of metal nanoparticle clusters, *Nat. Commun.* **5**, 3751 (2014).
- [13] J. R. Howse, R. A. L. Jones, A. J. Ryan, T. Gough, R. Vafabakhsh, and R. Golestanian, Self-motile colloidal particles: From directed propulsion to random walk, *Phys. Rev. Lett.* **99**, 048102 (2007).
- [14] I. Prigogine, Time, structure and fluctuations, *Science* **201**, 777 (1978).
- [15] L. P. Kadanoff, Turbulent heat flow: Structures and scaling, *Phys. Today* **54**(8), 34 (2001).
- [16] A. Y. Grosberg and J.-F. Joanny, Nonequilibrium statistical mechanics of mixtures of particles in contact with different thermostats, *Phys. Rev. E* **92**, 032118 (2015).
- [17] S. N. Weber, C. A. Weber, and E. Frey, Binary mixtures of particles with different diffusivities demix, *Phys. Rev. Lett.* **116**, 058301 (2016).
- [18] M. E. Cates and J. Tailleur, Motility-induced phase separation, *Annu. Rev. Condens. Matter Phys.* **6**, 219 (2015).
- [19] V. Dotsenko, A. Maciolek, O. Vasilyev, and G. Oshanin, Two-temperature Langevin dynamics in a parabolic potential, *Phys. Rev. E* **87**, 062130 (2013).
- [20] V. S. Dotsenko, A. Maciolek, G. Oshanin, O. Vasilyev, and S. Dietrich, Current-mediated synchronization of a pair of beating non-identical flagella, *New J. Phys.* **21**, 033036 (2019).
- [21] A. Y. Grosberg and J.-F. Joanny, Dissipation in a system driven by two different thermostats, *Polym. Sci., Ser. C* **60**, 118 (2018).
- [22] C. Battle, C. P. Broedersz, N. Fakhri, V. F. Geyer, J. Howard, C. F. Schmidt, and F. C. MacKintosh, Broken detailed balance at mesoscopic scales in active biological systems, *Science* **352**, 604 (2016).
- [23] J. Li, J. M. Horowitz, T. R. Gingrich, and N. Fakhri, Quantifying dissipation using fluctuating currents, *Nat. Commun.* **10**, 1666 (2019).
- [24] M. Wang and A. Y. Grosberg, Three-body problem for Langevin dynamics with different temperatures, *Phys. Rev. E* **101**, 032131 (2020).
- [25] H. Tanaka, A. A. Lee, and M. P. Brenner, Hot particles attract in a cold bath, *Phys. Rev. Fluids* **2**, 043103 (2017).
- [26] M. Wang, K. Zinga, A. Zidovska, and A. Y. Grosberg, Tethered tracer in a mixture of hot and cold Brownian particles: can activity pacify fluctuations? *Soft Matter* **17**, 9528 (2021).
- [27] E. Ilker, M. Castellana, and J.-F. Joanny, Long-time diffusion and energy transfer in polydisperse mixtures of particles with different temperatures, *Phys. Rev. Res.* **3**, 023207 (2021).
- [28] M. Jardat, V. Dahirel, and P. Illien, Diffusion of a tracer in a dense mixture of soft particles connected to different thermostats, *Phys. Rev. E* **106**, 064608 (2022).
- [29] C. Gardiner, *Handbook of Stochastic Methods for Physics, Chemistry and the Natural Sciences* (Springer, Berlin, 2004).
- [30] R. Livi and P. Politi, *Nonequilibrium Statistical Physics: A Modern Perspective* (Cambridge University Press, Cambridge, UK, 2017).
- [31] D. Chandler, J. D. Weeks, and H. C. Andersen, Van der Waals picture of liquids, solids, and phase transformations, *Science* **220**, 787 (1983).
- [32] See Supplemental Material at <http://link.aps.org/supplemental/10.1103/PhysRevResearch.6.013156> for additional numerical results for various values of the ratio of the diffusivities.
- [33] V. E. Debets, X. M. de Wit, and L. M. C. Janssen, Cage length controls the nonmonotonic dynamics of active glassy matter, *Phys. Rev. Lett.* **127**, 278002 (2021).
- [34] E. Irani, Z. Mokhtari, and A. Zippelius, Dynamics of bacteria scanning a porous environment, *Phys. Rev. Lett.* **128**, 144501 (2022).
- [35] M. Hidalgo-Soria, E. Barkai, and S. Burov, Cusp of non-Gaussian density of particles for a diffusing diffusivity model, *Entropy* **23**, 231 (2021).
- [36] S. Mandal, C. Kurzthaler, T. Franosch, and H. Löwen, Crowding-enhanced diffusion: An exact theory for highly entangled self-propelled stiff filaments, *Phys. Rev. Lett.* **125**, 138002 (2020).
- [37] J. Agudo-Canalejo, P. Illien, and R. Golestanian, Phoresis and enhanced diffusion compete in enzyme chemotaxis, *Nano Lett.* **18**, 2711 (2018).
- [38] H. Wang, M. Park, R. Dong, J. Kim, Y.-K. Cho, T. Tlusty, and S. Granick, Boosted molecular mobility during common chemical reactions, *Science* **369**, 537 (2020).
- [39] A.-Y. Jee, T. Tlusty, and S. Granick, Master curve of boosted diffusion for 10 catalytic enzymes, *Proc. Natl. Acad. Sci. USA* **117**, 29435 (2020).
- [40] M. Feng and M. K. Gilson, Enhanced diffusion and chemotaxis of enzymes, *Annu. Rev. Biophys.* **49**, 87 (2020).
- [41] A. Scala, F. Starr, E. La Nave, F. Sciortino, and H. E. Stanley, Configurational entropy and diffusivity of supercooled water, *Nature (London)* **406**, 166 (2000).
- [42] P. G. Debenedetti and F. H. Stillinger, Supercooled liquids and the glass transition, *Nature (London)* **410**, 259 (2001).
- [43] P. Charbonneau, Y. Jin, G. Parisi, and F. Zamponi, Hopping and Stokes-Einstein relation breakdown in simple glass formers, *Proc. Natl. Acad. Sci. USA* **111**, 15025 (2014).
- [44] S. Wei, Z. Evenson, M. Stolpe, P. Lucas, and C. A. Angell, Breakdown of the Stokes-Einstein relation above the melting temperature in a liquid phase-change material, *Sci. Adv.* **4**, eaat8632 (2018).
- [45] B. Doliwa and A. Heuer, Cage effect, local anisotropies, and dynamic heterogeneities at the glass transition: A computer study of hard spheres, *Phys. Rev. Lett.* **80**, 4915 (1998).
- [46] L. F. Cugliandolo, The effective temperature, *J. Phys. A: Math. Theor.* **44**, 483001 (2011).

- [47] S. Léonard and L. Berthier, Lifetime of dynamic heterogeneity in strong and fragile kinetically constrained spin models, *J. Phys.: Condens. Matter* **17**, S3571 (2005).
- [48] A. Heuer and K. Okun, Heterogeneous and homogeneous dynamics in a simulated polymer melt: Analysis of multi-time correlation functions, *J. Chem. Phys.* **106**, 6176 (1997).
- [49] S. Burov, S. M. A. Tabei, T. Huynh, M. P. Murrell, L. H. Philipson, S. A. Rice, M. L. Gardel, N. F. Scherer, and A. R. Dinner, Distribution of directional change as a signature of complex dynamics, *Proc. Natl. Acad. Sci. USA* **110**, 19689 (2013).
- [50] W. J. T. Bos, B. Kadoch, and K. Schneider, Angular statistics of Lagrangian trajectories in turbulence, *Phys. Rev. Lett.* **114**, 214502 (2015).
- [51] G. Ariel, A. Rabani, S. Benisty, J. D. Partridge, R. M. Harshey, and A. Be'er, Swarming bacteria migrate by Lévy walk, *Nat. Commun.* **6**, 8396 (2015).
- [52] B. Kadoch, W. J. T. Bos, and K. Schneider, Directional change of fluid particles in two-dimensional turbulence and of football players, *Phys. Rev. Fluids* **2**, 064604 (2017).
- [53] L. Fang, L. L. Li, J. S. Guo, Y. W. Liu, and X. R. Huang, Time scale of directional change of active Brownian particle, *Phys. Lett. A* **427**, 127934 (2022).